Published in final edited form as:

Nat Protoc. 2017 April ; 12(4): 732–747. doi:10.1038/nprot.2017.001.

Decerebrate mouse model for studies of the spinal cord circuits

Claire F Meehan[1,5], **Kyle A Mayr**[2,5], **Marin Manuel**[3], **Stan T Nakanishi**[4], **Patrick J Whelan**[2]

[1]Centre for Neuroscience, University of Copenhagen, Copenhagen, Denmark.

[2]Department of Comparative Biology and Experimental Medicine, University of Calgary, Calgary, Alberta, Canada.

[3]CNRS UMR 8119, Université Paris Descartes, Paris, France.

[4]Department of Biology, University of Hawaii at Hilo, Hilo, Hawaii, USA.

Abstract

The adult decerebrate mouse model (a mouse with the cerebrum removed) enables the study of sensory-motor integration and motor output from the spinal cord for several hours without compromising these functions with anesthesia. For example, the decerebrate mouse is ideal for examining locomotor behavior using intracellular recording approaches, which would not be possible using current anesthetized preparations. This protocol describes the steps required to achieve a low-blood-loss decerebration in the mouse and approaches for recording signals from spinal cord neurons with a focus on motoneurons. The protocol also describes an example application for the protocol: the evocation of spontaneous and actively driven stepping, including optimization of these behaviors in decerebrate mice. The time taken to prepare the animal and perform a decerebration takes ~2 h, and the mice are viable for up to 3–8 h, which is ample time to perform most short-term procedures. These protocols can be modified for those interested in cardiovascular or respiratory function in addition to motor function and can be performed by trainees with some previous experience in animal surgery.

INTRODUCTION

Over the past decade, the development of new genetic tools has induced a seismic shift in our knowledge of spinal cord circuitry[1–3]. These tools use transcription factor markers, which allow for discrete identification of sensorimotor circuits[4–7]. Indeed, when combined with optogenetic and pharmacogenetic approaches, they facilitate selective manipulation of populations of interneurons and motoneurons[8,9]. Several laboratories have demonstrated the ability to genetically dissect circuits using isolated neonatal spinal cord preparations[2,10].

Correspondence should be addressed to P.J.W. (whelan@ucalgary.ca).

AUTHOR CONTRIBUTIONS C.F.M., K.A.M., M.M., and S.T.N. performed the experiments, analyzed the data, and prepared figures. P.J.W. wrote the paper and edited figures. C.F.M., K.A.M., M.M., S.T.N., and P.J.W. conceived of the experiments. C.F.M., K.A.M., S.T.N., M.M., and P.J.W. edited the manuscript.

[5]These authors contributed equally to this work.

Note: Any Supplementary Information and Source Data files are available in the online version of the paper.

COMPETING FINANCIAL INTERESTS The authors declare no competing financial interests.

Elegant examples of targeted manipulation of neuronal populations, including motoneurons, have been published using these useful preparations. Yet these studies also highlight a critical gap in our knowledge. Although studies of these isolated young spinal cord preparations have produced enlightening results in perinatal motor control, there has been less work concentrating on the adult mouse spinal cord. There is a disconnect between perinatal mouse models used to examine circuits and the adult mouse, in which generally only behavior can be examined[11]. Spinal circuits are still developing perinatally, and weight support occurs only after the first neonatal week. Indeed, receptor densities, descending tracts, proprioceptive feedback during weight support, and spinal circuits are examples in which changes occur during development[12–15].

Development of the technique

The development of the decerebrate mouse (a mouse with the cerebrum removed) follows logically from the use of *in vivo*-anesthetized mouse preparations[16–18]. It was driven by a desire to record both fictive locomotion and stepping behavior, which were not possible using the anesthetized preparation. Although decerebrate animals have been studied in many species, the mouse posed particular challenges due to its small size. Size is important because of the greater surface area to volume ratio of smaller mammals and the subsequent risk of heat loss. Furthermore, as metabolic rate per kilogram is inversely proportionate to the total weight of the animal, mice have higher ventilatory rates, heart rates, and heat loss[19]. As the average blood volume of a mouse is ~75 ml/kg, and the range of weights for standard C57/B6 mice is between 10 g (3 weeks old) and 30 g, the blood volumes are limited to 750 μl–2.25 ml. Therefore, the maintenance of decerebrate mouse preparations requires careful attention to ventilation rates during anesthesia, episodes of blood loss, and temperature regulation. We outline the step-by-step procedure for surgically preparing a decerebrate mouse with minimal blood loss, allowing recordings to be taken for many hours. These adaptations to a traditional decerebrate preparation are necessary because of the small size of the mouse. This allows invasive experiments to be designed that could not be performed on conscious mice.

Overview of the procedure

We describe methods to record neuronal signaling *in vivo*, which can be difficult because of the small size of the mouse. We bring together a coordinated set of protocols from three laboratories, in Denmark, France, and Canada, to apply a best-practices approach to describing this preparation. The first set of experiments using these preparations and intracellular approaches have been published[16–18,20–26], and therefore this is an opportune time to describe the protocol in detail so that it can be applied in other laboratories.

Advantages and limitations

Current models for studying the spinal sensory-motor system in adults have been largely limited to anesthetized preparations. A substantial limitation of such models, however, is that anesthetics themselves alter the excitability of the neurons by suppressing various conductances, such as persistent inward currents. Not only can this confound results regarding intrinsic neuronal excitability, but the use of different anesthetics can make it difficult to compare results across laboratories. Our decerebrate model therefore provides a

major advantage over existing models in that the intrinsic properties of motoneurons can be measured unaffected by anesthetics. The other major advantage of our decerebrate model is that it is possible to activate spinal central pattern generators (CPGs) such as that for locomotion[20,21], which is not possible in anesthetized mice[21]. Previously, investigations of this spinal circuitry in mice have been limited to neonatal preparations. Being an adult model, our decerebrate preparation allows for investigations of the mature spinal circuitry of the CPGs using transgenic and optogenetic technology. Adult mouse decerebrate models also have advantages for investigating neuronal excitably and connectivity in adult-onset motoneuron diseases such as amyotrophic lateral sclerosis (ALS). The model can also be adapted for use in all segments of the spinal cord and in both the dorsal and ventral horns, extending the potential use of the model to many fields.

The main limitation is that it requires greater technical expertise than *in vitro* electrophysiological approaches. A higher premature mortality will initially be observed as compared with anesthetized *in vivo* preparations; however, this can be reduced substantially with practice. In addition, as compared with that of behaving awake animals, the behavioral repertoire of decerebrate mice is limited. Finally, as they are decerebrate, these preparations can be used only acutely and are not suitable for chronic long-term procedures. These limitations should be kept in mind when considering the adoption of the decerebrate model.

Applications

The biological application of the adult decerebrate *in vivo* mouse provides a preparation in which to study sensory-motor integration and motor output from the spinal cord in control and transgenic adult mice without compromising these functions with anesthesia. For example, the ability to study the modulation of chronic neuropathic pain at a cellular and systems level using electrophysiological methods in a transgenic *in vivo* model is now possible. We are also able to measure kinematic data about limb position and angles at various speeds of locomotion, and we are in the process of applying optogenetic methods to modulate the activity of identified descending neuromodulatory projections and their effects on locomotion. Furthermore, a number of transcription factors and genetic markers have been identified and associated with subsets of interneurons in the spinal cord. Using this information, it will be possible to experimentally manipulate various subsets of interneurons *in vivo*.

We use examples of locomotion as a spinally coordinated behavior to demonstrate the application of this model, and include an example of photostimulation of $VGAT^{+}$ neurons to illustrate its use. Beyond sensory-motor functions, however, the decerebrate mouse preparation can be used in other areas of research, including studies of spinal cord injury, multiple sclerosis, respiratory physiology, cardiovascular function, and muscle physiology.

Alternative methods

Examining adult spinal cord motor function with *in vitro* preparations is more difficult than doing so in neonates. The crux of the issue is the requirement to maintain the viability of adequate amounts of spinal cord tissue to allow distributed motor networks to function[27]. Adult spinal cord slice approaches provide a complementary method for

studying intrinsic and synaptic properties of identified neurons[28], but only thin slices of spinal cord can be kept alive for recording interneuron and motoneuron spike activity[29,30]. An alternative approach is the use of *in vitro* adult sacral spinal cord tissue with multiple intact segments[31–33]. Anesthetized *in vivo* preparations are another alternative for labs that are initiating attempts at *in vivo* experiments. However, these approaches are not appropriate for studying locomotor behavior. By using *in vivo* decerebrate approaches, neurons can be examined in a more physiological relevant state, with descending projections and sensory input left intact. Correlations between behavior such as locomotion and neural activity in the same *in vivo* system are also possible. We believe that the decerebrate mouse model provides a complementary preparation that can be combined with the alternative methods listed here to build a comprehensive overview of motor function.

Experimental design

As pointed out above, blood loss is an important concern for mouse preparations. For these reasons, we would highly advise researchers to consider using anesthetized mice[16,17] to learn intracellular recording before adopting the decerebrate procedure. This allows trainees to practice their surgical skills and collect intracellular recording data in anesthetized preparations before moving on to the protocol outlined here.

Researchers adopting the decerebrate preparation need to ensure that the preparation is kept hydrated to compensate for blood loss. Once established, the preparation is quite stable; however, control experiments need to be run to ensure that bouts of locomotion or motor activity are stable over the proposed duration of the experiment. This will help ensure that any experimental manipulation is not occurring over a backdrop of preparation run-down.

The Axoclamp 2B (no longer sold by Molecular Devices—but available second-hand) is used by investigators here and is preferred due to its ease in manipulating current injection and other parameters during sharp recordings. We have listed the Multiclamp 900A as an alternative, but the responsiveness of the analog interface of the Axoclamp 2B is better for *in vivo* recordings for which adjustments need to be performed in the process of data collection.

This protocol describes steps to create a fictive or actual stepping preparation. A fictive preparation is ideal for making intra-axonal or intracellular recordings. One could use these preparations to examine changes in afferent transmission or changes in intrinsic firing properties of neurons in the spinal cord. On the other hand, stepping preparations are ideally suited to examining behavioral output of the network. Afferent inflow remains intact and can be manipulated to examine changes in locomotor function. Motor output can be measured by directly recording muscle electromyo-grams (EMGs), kinematics, or force. In some cases, both preparations can be used. For example, if the effects of afferent inflow were being manipulated, it would be advantageous to test this in a stepping preparation to examine changes in behavior. These could be compared and contrasted with fictive locomotion in which mechanisms of action could be addressed at a cellular level. Figure 1 presents a flowchart of the procedure.

MATERIALS

REAGENTS

- Mice: C57BL/6J (JAX Mice Strain; Charles River, cat. no. 000664) or Swiss Webster Crl:CFW(SW) (CFW; Charles River) **! CAUTION** All experiments should be performed in accordance with relevant guidelines and regulations. The following local ethics committees approved all procedures described here: the University of Calgary Health Sciences Animal Care Committee (Canadian Council of Animal Care guidelines), the Paris Descartes Ethics Committee (CEEA34.MM.064.12), and the Danish Animal Experiments Inspectorate (Dyreforsøgtilsynet; permission nos. 2012-15-2934-00501 and 2015-15-0201-005450. All procedures were performed in accordance with EU Directive 2010/63/EU. Guidance regarding decerebrate animals not perceiving pain should be provided by the relevant institutional animal care and use committee (US)[34]. Where applicable, refer to local guidelines. ▲ **CRITICAL** We have used two strains of mice in our decerebrate experiments: Swiss Webster (CFW) and C57BL/6. The C57BL/6 is the most popular strain of mouse used, as it forms the background strain for many transgenic lines. We did observe some differences in the quality of stepping produced, with the CFW strain producing more consistent actual stepping. For intracellular recording, however, we were able to record consistent fictive steps with C57BL/6 animals.
- Isoflurane USP (Fresenius Kabi) **! CAUTION** Halogenated gases can cause dizziness, nausea, eye irritation, and headache. Long-term effects are not fully known. Leakage of isoflurane usually occurs from nose cone and the induction box. The induction box should be used in a fume hood, and gases escaping the nose cone should be vented to a fume hood.
- Medical-grade oxygen—for vaporized anesthetic (100% medical grade, tank grade: 1072; Praxair)
- 95% (vol/vol) isopropyl alcohol/5% DiO_2 (vol/vol) (MilliporeSigma, cat. no. PX1830-4)
- Ophthalmic gel (Optixcare Eye Lubricant; CLC Medica)
- Mouse intubation cannula (Harvard Apparatus, model no. VK32(73–2844))
- Braided silk suture thread, needle unattached, 4-0 (Ethicon, cat. no. SA83H)
- Braided silk suture thread, needle unattached, 6-0 (Fine Science Tools, cat. no. 18020-60)
- Suture needles, nonthreaded (Fine Science Tools, cat. no. 12050-03)
- Rounded diamond-embedded burr bit (Hager & Meisinger, model no. IRF-009)
- Glass micropipettes (Harvard Apparatus, borosilicate glass electrodes with filament GC120F-10, cat. no. 30-0044 or GC150F-10, depending on your electrode holder)

- Absorbable hemostat strip (Surgicel; Ethicon, cat. no. 63713-0019-55) ▲ **CRITICAL** Surgicel should be cut into strips that can be easily inserted into the skull during decerebration.
- Bone wax (SMI, cat. no. Z046)
- Sterile lactated Ringer's solution (Braun Medical, cat. no. L7501)
- 23-Gauge needle (PrecisionGlide IM; BD, cat. no. 305145)
- 30-Gauge half-inch needle (PrecisionGlide IM; BD, cat. no. 305106)
- 35-Gauge, 3-strand Teflon-coated stainless steel wire (A-M Systems, cat. no. 793400)
- Cotton-tipped applicator (VWR International, cat. no. 89031-270)
- Gauze sponge (Professional Preference, cat. no. 110808)
- No. 10 round stainless steel surgical blade (Integra Miltex, cat. no. 4–310)
- aCSF (128 mM NaCl, 4 mM KCl, 1.5 mM $CaCl_2$, 1 mM $MgSO_4$, 0.5 mM Na_2HPO_4, 21 mM $NaHCO_3$, 30 mM D-glucose) ▲ **CRITICAL** Alternatively, Ringer's solution (Sigma-Aldrich, cat. no. 96724) can be used.
- Intrathecal catheter (Alzet, cat. no. catheter MIT-02)
- Vetbond surgical glue (3M Canada, cat. no. 1469SB)
- Kwik-Cast Sealant (WPI, cat. no. Kwik-Cast)
- Pancuronium bromide (Sigma-Aldrich, cat. no. P1918)
- Monoamine oxidase inhibitor, nialamide ▲ **CRITICAL** This monoamine oxidase inhibitor has been shown in cats to reduce dopamine metabolism and therefore potentiate the effect of L-DOPA 34–36. This is best administered in two doses of 100 mg/kg with at least 1 h in between doses, at least 2 h before surgery commences.

EQUIPMENT

Surgical tools

- Extra-fine Graefe Forceps (Fine Science Tools, cat. no. 11152-10)
- Extra-fine Graefe toothed forceps (Fine Science Tools, cat. no. 11154-10)
- 5/45 Forceps (Fine Science Tools, cat. no. 11251-35)
- Needle driver with inset scissor (Fine Science Tools, cat. no. 12002-12)
- Microscissors (Fine Science Tools, cat. no. RS-5620)
- Rongeurs (Fine Science Tools, cat. no. 16221-14)
- Dumont no. 2 laminectomy forceps (Fine Science Tools, cat. no. 11223-20)

- Curved spatula, length: 6.25 inches (16 cm; Fisher, cat. no. 21-401-25A) This can also be custom-made from a simple small metal spatula (Supplementary Fig. 1a)

Other equipment—▲ CRITICAL Update equipment to newer versions as appropriate.

- Isoflurane vaporizer (SurgiVet Vaporizer; Smiths Medical, model no. 100)
- Mouse respirator (Minivent; Harvard Apparatus, model no. 845)
- Wireless hair trimmers (Wahl Industries, model no. 9960)
- Hand-held cauterizer tool (Acu-Tip Portable; Practicon, model no. 7051711)
- High-speed micro-drill (Stoelting, model: Ideal micro 2953)
- Stereotaxic frame with ear bars (Stoelting, model no. 51625 or Narashige, model no. STS-A)
- Compact spinal cord clamps (Narashige, model: Narashige STS-A) or, alternatively, Cunningham spinal stereotaxic adaptors (Harvard Apparatus, model no. 51690). The recordings shown in this article were made using the Narashige clamps. Narashige vertebral clamps limit the working space above the mouse but offer the flexibility of clamping larger regions, tilting the cord and stretching the vertebrae slightly to reduce movement and improve stability
- Custom-made leg holder (Supplementary Fig. 1b)
- Temperature-controlled variable heat lamp, 100W (Leviton Manufacturing)
- Temperature-controlled variable heat pad (K&H Manufacturing, model no. 1009)
- Rectal thermal probe (Raytek Thermalert, model no. TH-5 or CWE, model no. TC-1000)
- Extracellular recordings headstage (Dagan Instruments, model no. 4001)
- Amplifier (Dagan Instruments, model no. ex4-400 or Digitimer Neurology System)
- Digitizer (Power 1401, CED, or Digidata 1550, Molecular Devices)
- Force transducer (UFI, model no. 1030)
- Carbon dioxide air measurement system (MicroCapstar End-tidal CO_2 analyzer, CWE)
- Analysis software (Spike 2, CED or Clampex/Clampfit 10, Molecular Devices or MatLab, MathWorks)
- Intracellular amplifier (Molecular Devices, model: Multiclamp 900A or Axon Instruments, model: Axoclamp 2B)
- Micropipette puller (Sutter Instruments, model no. P-97)
- Stepper motor (Micropositioner, Kopf, model no. 2660)

Locomotor treadmill for experiments with stepping locomotion

- Half-inch Plywood (Home Depot Canada, cat. no. 894001020)
- 2-inch-thick polystyrene sheet (Rona, cat. no. 0510004)
- Abec 5 1/2 -inch ball bearing (Rona, cat. no. 0696094) 3/8-inch threaded stainless steel rod (Home Depot Canada, cat. no. 5091-318)
- Lego Mindstorms NXT Kit (LEGO, cat. no. 8547)
- 8-inch-circumference rubber bands (Staples Canada, cat. no. 39380)
- Stereotaxic facial holder (Stoelting, cat. no. 51629)
- Adjustable-height bar (Home Depot Canada, cat. no. 801637)

PROCEDURE

Induction of general anesthesia ● TIMING 10 min

1. Administer nialamide in two doses of 100 mg/kg with at least 1 h in between doses at least 2 h before surgery commences. This step is required for fictive locomotion only.
2. Place the mouse in a sealed induction chamber with 1 ml of isoflurane (1-chloro-2,2,2-trifloroethyldifluoro-methyl ether, PPC) added to a small cloth at the bottom.
3. Verify that the mouse is in an anesthetized state by checking the righting reflex by tilting the induction chamber. The righting reflex is defined as the mouse's ability to turn right side up after being flipped over. Check the anesthetized state by testing withdrawal reflexes to toe and tail pinch.
4. After verification of complete anesthesia, put the mouth and nose into a nose cone delivering 2–2.5% (vol/vol) isoflurane with oxygen (medical-grade oxygen) at 0.4 l/min. The amount of anesthesia required will vary per mouse, but normally it needs to be adjusted to between 1.5 and 2.0%. Throughout the procedure, withdrawal reflexes should be periodically tested. Ventilation rates can vary from a low of 72 breaths/min for fictive locomotion to a high of 168 breaths/min for actual walking.

   ▲ **CRITICAL STEP** Look for irregularities in breathing; isoflurane at desired levels will slightly reduce the breathing rate.

   ? TROUBLESHOOTING

Carotid artery ligation and intubation ● TIMING 30 min

5. Place the mouse on its dorsal side on a covered, heated pad. Lightly tape the forelimbs to the table to allow for stability and better surgical access.
6. Shave the skin around the trachea with a pair of small hair clippers, and remove excess fur using 95% (vol/vol) isopropyl alcohol on a piece of gauze.

7. Using a round-tip 10-mm scalpel blade, make an incision on the skin midline from the sternum to the trachea, moving rostrally toward the bottom of the jaw (Fig. 2a,b).

8. Isolate the left and right carotid arteries via blunt dissection using the extra-fine Graefe forceps along with the 5/45 forceps (Fig. 2c).

   ▲ **CRITICAL STEP** The vagus nerve runs parallel to the carotid artery; it must be separated before ligation, with extra care taken not to damage it via cutting or crushing.

9. Dissect the vagus nerve away from the carotid artery and exclusively tie off the artery using 6-0 suture thread (Fig. 2c–e).

   ▲ **CRITICAL STEP** The carotid arteries are fragile; use caution when tying these off. Two ligation sutures are recommended to completely occlude blood flow.

   ? TROUBLESHOOTING

10. Expose the trachea with blunt dissection of the sternohyoid muscle, located ventrally to the trachea, to expose the cartilage rings of the trachea (Fig. 2f,g).

11. Run two lengths of 4-0 suture thread underneath the trachea to the opposing side (Fig. 2h).

12. Using microscissors, perform a tracheotomy by cutting a small incision between two pieces of cartilage horizontal to the trachea; the incisions should be large enough to allow insertion of the stainless steel endotracheal tube (Fig. 2i).

    ? TROUBLESHOOTING

13. Insert the tube ~1–2 cm through the dissected tracheal incision.

    ▲ **CRITICAL STEP** This process must be completed quickly to ensure that the mouse does not wake up during the procedure. It is important to increase the anesthetic level slightly beforehand to allow more time for the cannulation procedure.

    ? TROUBLESHOOTING

14. Secure the tracheal tube in place by using the two nylon 4-0 sutures previously run underneath the trachea and securing with square knots. Close the incision using nylon suture thread and standard interrupted suturing techniques (Fig. 2j).

    ▲ **CRITICAL STEP** After intubation, reduce the anesthetic level while maintaining a lack of reflex response to tail pinch and whisker stimulation.

    ? TROUBLESHOOTING

Laminectomy or intrathecal application ● TIMING 30 min

15. Shave the head and lower back, as well as the left side of the mouse, completely to minimize fur entering the open incisions. Make a superficial cut ~3 cm in length along the midline of the spine around the end of the fat pad (T8–T9).

16. Blunt-dissect the connective tissue to expose the vertebra of interest completely (Fig. 3a).

17. With the vertebra fully exposed, remove the top portion of the vertebra with rongeurs or laminectomy forceps to expose the spinal cord. If required, extend the laminectomy across several sections to create an elongated well for direct drug application (Fig. 3a–d).

? TROUBLESHOOTING

18. Administer drugs by performing a lumbar laminectomy pool (option A) or intrathecal catheter subdural insertion (option B). Option A is preferred for intracellular recordings, and option B is preferred for stepping experiments.

▲ **CRITICAL STEP** Some drugs do not pass through the blood–brain barrier; therefore, for many drugs intrathecal application is required. For these applications, it is important to fully remove the dura (obligatory for intracellular recording experiments).

A. Drug application pool in lumbar laminectomy

i. Remove the dura by using a 30-gauge needle to create a cut horizontal to the spinal cord, creating a small incision. Through this hole, lift the dura with the 5/45 microforceps and use the microscissors to cut the dura and expose the spinal cord (Fig. 3a).

▲ **CRITICAL STEP** When the spinal cord is exposed, it is critical not to let it dry out. Always keep it well saturated with gauze soaked in aCSF or Ringer’s solution.

ii. Place the mouse within a stereotaxic frame by securing ear bars into ear canals and placing the mouth into a tooth holder for stability.

iii. For intracellular recordings, form a pool of mineral oil on top of the spinal cord. This is done in one of two ways, depending on the spinal clamps used. When using Narashige vertebral clamps, tie and extend the skin dorsally with silk threads (Fig. 4a). Tie the threads to the frame to create a mineral oil pool. If you are using Cunningham spinal stereotaxic adaptors, clamp the spinal column from the lateral aspects, which has the advantage of more working space dorsal to the cord. For these adaptors, use a custom-made plastic pool and suture the skin flaps to it.

Next, render the plastic pool leak-proof by applying Kwik-Cast sealant (WPI). Once the sealant has cured (5 min), pour mineral oil over the spinal cord (Fig. 4b).

B. Intrathecal catheter subdural insertion

i. Create a small incision in the dura by using a 30-gauge needle to create a cut horizontal to the spinal cord.

ii. Fill and moisten the catheter with aCSF.

iii. Run the catheter s.c. through an opened skin incision from the midline between the left and right scapula down to the laminectomy site.

iv. Insert the catheter, subdurally and parallel to the spinal cord, into the previously opened dural incision and slide caudally toward the region of interest of the spinal cord.

v. Secure the catheter at the laminectomy site with a small drop of Vetbond on the skin, taking extra care not to contaminate the laminectomy site. Secure the rostrally facing end of the catheter to the skin by two interrupted sutures through the skin if desired.

19. If you wish to perform nerve dissection for intracellular recordings and fictive locomotion, follow the procedure described in Box 1 and illustrated in Figures 5 and 6. Otherwise proceed to the next step.

Craniotomy and decerebration ● TIMING 30 min

20. Shave and clean the head with 95% (vol/vol) isopropyl to remove excess hair.

21. Make a superficial cut across the midline of the skull, along its entire length, in the rostral-to-caudal direction.

22. Score the skull on the lambda and bregma fissures with a microdrill and rounded burr bit as in Figure 7.

▲ **CRITICAL STEP** It is not necessary to penetrate the bone—rather, lightly score to create weak spots for complete and easy removal.

23. Remove the skull with rongeurs, exposing the brain and resulting square field ~1–2 mm caudal to the lambda and 1–3 mm rostral to the bregma and extending perpendicular to the midline roughly 1–2 cm to the left and right sides of the midline (Fig. 7b).

? TROUBLESHOOTING

24. Perform the decerebration resection with a surgical scalpel (no. 10 blade; Fine Science Tools or the custom-made tool, Supplementary Fig. 1a) at the previously existing lambda crest at a 45° angle. Make the incision from the dorsal section of the brain ventrally at a 45° angle, with the blade perpendicular to the midline, in

a quick slicing motion across the horizontal plane (Fig. 7b). The goal is to end with a premammillary decerebrate preparation.

▲ **CRITICAL STEP** Try to keep the mammillary bodies as intact as possible, as this will aid in both viability and successful spontaneous stepping (in case of a stepping preparation).

25. Remove the rostrally separated section by using a small curve-bladed microspatula. Fill the hole with Surgicel strips to help keep bleeding to a minimum and fill the newly formed space.

▲ **CRITICAL STEP** It is critical to curtail bleeding; make sure that the tools are ready for resection of the cerebrum and that hemostatic Surgicel is ready to be inserted into the skull.

26. Suture the skin on the skull using interrupted suturing techniques for stepping preparations.

▲ **CRITICAL STEP** For experiments that use drugs that increase blood pressure, such as L-DOPA, it is useful to leave the area exposed to monitor for fresh bleeding. If this occurs, add fresh Surgicel to the skull cavity.

27. Once the bleeding has subsided, remove the Surgicel and confirm the completeness of the decerebration before removing the isoflurane anesthetic from the flow.

▲ **CRITICAL STEP** For fictive locomotion experiments, it is necessary to allow at least 40 min for the isoflurane to be metabolized before administering L-DOPA. For intracellular recording of intrinsic properties of neurons, it is advised to wait for at least 1 h after removal of the anesthetic to ensure that reliable data are obtained.

Data acquisition

28. *Acquisition of data*. Follow option A for fictive locomotion experiments and option B for stepping experiments.

A. Fictive locomotion experiments ● TIMING 10 min

i. *Preparation for intracellular recordings*. Administer the neuromuscular blocking agent pancuronium bromide to prevent movements (dilute 1:10 with saline and then give a 0.1-ml dose i.p. initially, followed by 0.05-ml doses every hour).

ii. Place a monopolar recording electrode on the surface of the spinal cord. Place the reference electrode on a muscle near the vertebral column. Connect this recording electrode to an AC amplifier (bandwidth: 10 Hz–5 kHz). This electrode is used to record the afferent volley reaching the spinal cord ~1 ms

after electrical stimulation of the sciatic nerve (or one of its branches).

? TROUBLESHOOTING

iii. Stimulate the hind limb nerve with a 50-μs pulse of supra-maximal intensity at a frequency of 1–5 Hz.

iv. By slowly moving the recording electrode along the spinal cord rostro-caudally, identify the region where the afferent volley is at a maximum. This corresponds to the area in which the density of motoneurons is the highest. Make a patch in the pia at this level with the extra-fine Graefe forceps.

v. Using a stepper motor, bring an intracellular electrode into contact with the spinal cord. Using an approach through the dorsal columns, angle the electrode 10–15° from the vertical and point it toward the lateral part of the spinal cord to reach the lateral motoneuron pools in the ventral horn.

vi. Drive the microelectrode through the dorsal part of the spinal cord.

▲ **CRITICAL STEP** Care should be taken to avoid compressing the spinal cord at this point.

vii. Throughout the track, use a small pulse of current to monitor the resistance of the electrode (which should have been zeroed at the surface of the spinal cord using the bridge balance knob of the amplifier). The resistance of the electrode increases when in contact with a cell.

▲ **CRITICAL STEP** The shape of the electrode and its impedance is critical for successful intracellular recordings. We routinely use KCl-filled glass micropipettes pulled to an ~1-μm tip with a resistance of 10–15 MΩ or 2 M potassium acetate with a resistance of ~25 MΩ (or lower for voltage clamp).

viii. Once the electrode is ~800 μm deep, drive the electrode using 3- to 6-μm steps.

ix. Track for motoneurons up to a depth of ~1,500 μm. Observe the electrode potential recording after each electrical stimulation of the nerve. When close to the motoneuron pool innervating the stimulated nerve, this stimulation elicits a distinctive field potential (visible as a downward deflection on the electrode potential recording). If no field potential is observed in response to nerve stimulation, bring the electrode back out of the spinal cord, and move the electrode 50–100 μm in either the rostro-caudal direction or the mediolateral

direction. Repeat Step 28A(ii–ix) until a field potential is observed.

? TROUBLESHOOTING

x. Identify motoneurons by the invasion of an antidromic action potential following the electrical stimulation of the nerve. Following impalement and identification, apply a series of protocols to characterize the electrical properties of the motoneuron (see ANTICIPATED RESULTS and Fig. 8). Methods for intracellular recordings are described in detail in previous work[16,17]. To measure the after-hyperpolarization (AHP), a short depolarizing current pulse of 1 ms can be applied through the microelectrode (using bridge mode on the Axoclamp amplifier) and successive trials can be averaged (using the Spike 2 software). Repetitive firing can be achieved in two ways. The first method uses short (500 ms) square current pulses of progressively stronger current intensities injected into the cell body through the microelectrode (with the Axoclamp amplifier in discontinuous current (DCC) mode). The steady-state firing frequency can be measured and plotted against the current intensity to obtain the *I–f* gain for the neuron. Alternatively, triangular depolarizing–repolarizing current ramps can be used to elicit repetitive firing (also in DCC mode) and the instantaneous firing frequencies (calculated by the Spike 2 software) are plotted against the current intensity. This second method allows for a faster acquisition of the data needed to calculate the *I–f* gain and allows for a fast comparison of recruitment versus de-recruitment current intensities to test for the presence of persistent inward currents. The disadvantage of using triangular current ramps is that persistent sodium currents are activated on the ascending ramp before reaching the threshold for the action potential. Measurements for voltage threshold and rheobase are therefore more accurately obtained using square current pulses of increasing intensity. A series of small-amplitude (−3 to +3 nA), 500-ms square current pulses (in DCC mode) can be used to plot the *I–V* relationship.

? TROUBLESHOOTING

B. Stepping experiments ● TIMING up to 2 h 20 min

i. *Force transducer setup for estimating weight-support during walking*. Make a small incision of 1 cm along the midline above the sacrum in the rostro-caudal direction.

ii. Thread a suture through the gluteal muscle or the skin perpendicular to the midline of the body with 4-0 suture thread.

iii. Tie a knot in the end of this thread, creating a loop. Attach the force transducer through the main force blade hole, securing it with three overhand knots.

iv. Calibrate the force transducer by adjusting the variable resistor until the baseline rests at zero.

v. *EMG hook electrode implantation for actual stepping experiments*. Thread 12–16 inches of 35-gauge, three-strand, Teflon-coated stainless steel wire through the lumen of the 23-gauge needle (Supplementary Fig. 1c).

vi. Strip 2–3 mm of the Teflon coating from the end closest to the bevel of the needle (Supplementary Fig. 1d).

vii. Fold the 2-mm end 180° (parallel to the existing wire) and pull it into the lumen (Supplementary Fig. 1e,f).

viii. Repeat Step 28B(v–vii) as needed; two wires are required for each muscle group for recording.

ix. Insert two wires into each muscle for recording. Place one wire distally in the muscle and one located more proximally.

x. While withdrawing the needle, rotate slowly clockwise and counterclockwise, leaving the hooked wire implanted inside the muscle.

xi. *Obtainment of locomotor recordings*. Using these methods, recordings can be obtained for 1–2 h. After this period, euthanize the mouse using sodium pentobarbital.

? TROUBLESHOOTING

Troubleshooting advice can be found in Table 1.

● **TIMING**

For surgery on a single decerebrated mouse:

Steps 1–4, induction of general anesthesia: 10 min

Steps 5–14, carotid artery ligation and intubation: 30 min

Steps 15–19, laminectomy and intrathecal preparation: 30 min

Steps 20–27, craniotomy and decerebration: 30 min

Steps 28A(i–x), preparation for intracellular recordings: 10 min

Steps 28B(i–iv), force transducer setup: 5 min

Steps 28B(v–x), EMG hook electrode implantation: 15 min

Step 28B(xi), locomotor recording and euthanization: up to 2 h

Box 1, nerve dissection for intracellular recordings and fictive locomotion: 15 min

ANTICIPATED RESULTS

Intracellular recordings

We can attest that following the described procedure decerebrate preparations can be maintained for up to 8 h after decerebration, during which time it is possible to obtain intracellular recordings of a quality similar to those we observe in anesthetized mouse preparations (Figs. 8 and 9). Stable recordings can be obtained, allowing measurements of all the intrinsic properties of motoneurons, including features of single action potentials such as AHP, rheobase, and voltage threshold for the action potentials; input resistance; and repetitive firing behavior such as current-firing frequency slope. We have successfully used similar techniques in anesthetized mice (up to 750 d old) to investigate the intrinsic properties of spinal motoneurons both in normal mice[16,17,22] and in transgenic models of the diseases affecting motoneurons, such as ALS[18,23,24] and Charcot–Marie Tooth disease[25], and we anticipate that the decerebrate preparation will expand the questions that can be asked in aged and diseased mouse models. We have also applied these intracellular recording techniques in the decerebrate mouse model to study the firing activity of spinal neurons during fictive locomotion and fictive scratch activity[20,21], as well as that of afferents using intra-axonal dorsal root recordings[20].

To demonstrate that the motoneurons in the decerebrate preparations are healthy, we compared the *I–f* gains (in the primary range) of motoneurons in decerebrate mice with those of mice anesthetized with different anesthetics: fentanyl citrate (Hypnorm) and midazolam, ketamine and xylazine, and sodium pentobarbital (while keeping all other parameters, such as ramp speed, constant). The results of this demonstrate that motoneuron health was not affected by the decerebration; in fact, successful intracellular penetrations of motoneurons displaying repetitive firing within these ranges could be obtained up to 8 h after the decerebration. The main difference with the *I–f* gain in the decerebrate occurs with respect to the secondary range, which reflects the onset of persistent inward currents, presumably originating in proximal dendrites from activation of L-type calcium channels[35]. Here we see that in the decerebrate preparations the transition from primary to secondary range occurs earlier than in anesthetized preparations. The fact that the secondary range is so pronounced in the decerebrate is consistent with descending monoaminergic innervation in the decerebrate preparation.

One of the remaining limitations of intracellular recording in mice is the technical difficulty of recording from interneuronal populations. Although difficult, it is possible, and over the years we have obtained a small sample of ventral horn candidate interneuron recordings (Fig. 8b,d,e). As with larger animals, these can be identified by a combination of criteria, including location/depth, a lack of antidromic activation, a distinctive high-frequency injury discharge on initial penetration, high firing frequencies, steep *I–f* slopes, and short AHPs. The AHP durations and *I–f* slopes of interneurons such as that illustrated in Figure 8 are

well outside of the range that we have recorded in antidromically identified motoneurons in both anesthetized and decerebrate preparations over the years. To demonstrate this, we have illustrated the *I–f* slope of the interneuron in Figure 8d along with an average *I–f* slope from a mouse motoneuron and the steepest *I–f* slope we have ever recorded from a mouse motoneuron. Because of the small size of the mouse spinal cord, however, antidromic identification of descending or ascending axons is complicated by stimulus spread even at low stimulation intensities.

One can not only record in current clamp; voltage-clamp recordings are also possible using sharp microelectrodes. We have achieved this *in vivo* by using a device developed by R. Lee (Emory University) and C.J. Heckman (Northwestern University)[36,37]. The device is connected to an intracellular amplifier (e.g., Axoclamp 2B) and acts as an external feedback loop to enhance low-frequency gain, which allows for an increase in gain without the high-frequency oscillations or ringing that can occur in voltage-clamp, particularly those using sharp microelectrodes. Using this setup, we can record voltage-clamp synaptic events such as excitatory postsynaptic currents (EPSCs), as shown in Figure 8. By incorporating step protocols that increase voltage, one can obtain measurements of the *I–V* relationship or one can use gradually increasing voltage ramps that are helpful in detecting persistent inward currents (Fig. 8). We can observe the onset of a negative region at ~−53 mV, showing the onset of a persistent inward current, which can be detected by measuring the deviation of the negative slope region from the theoretical line expected without activation of a persistent inward current (Fig. 8h)[38].

Fictive stepping preparation

Fictive locomotion can be elicited from mice, and reliable patterns can be recorded from muscle nerves innervating muscles of the hind limbs. After our decerebration, the appearance of spontaneous fictive locomotion is rare. We usually wait ~40 min for the anesthetic to leave the system before we try to evoke locomotion with drugs. Our previous work established that i.p. administration of L-DOPA facilitated these bouts of locomotion[21].

We have found that locomotion is evoked with dosages of L-DOPA as low as 2 mg for a 25-g mouse (80 mg/kg)[21]. Rhythmic activity usually starts as slow synchronous activity on all nerves, and then gradually the frequency of the rhythm increases and alternates between the left and right sides and flexor and extensor electroneurograms (ENGs) (Fig. 9). In our current experiments, we have found that at this point the pattern is improved by the administration of 25 μg of 5-hydroxytryptophan (5-HTP). Eventually, the rhythmic activity starts to become less robust, the frequency decreases again and becomes synchronous. Here we have found that another 25-μg dose of 5-HTP restores the rhythm.

Rhythmic activity can also be activated by spinalization (Fig. 10). This can improve the quality of ongoing L-DOPA-elicited locomotor activity—by speeding up and improving alternation—and also induce activity when none has been achieved by L-DOPA alone or when it has started to fail (Fig. 10b). This effect is usually fairly short-lived, and thus to test whether it was just the release from inhibition or that we were stimulating descending pathways with the lesion, we performed 2 lesions. This is shown in Figure 10b. After the first cervical lesion, fictive locomotor activity is evoked. After the rhythm ceases, it can

be reinitiated by a thoracic lesion. We have also shown that peripheral nerve stimulation can elicit rhythmic activity in L-DOPA-treated mice before a sustained episode of L-DOPA-evoked locomotion begins (Fig. 9b). Furthermore, we confirmed that stimulation of the peripheral nerves can reset an ongoing L-DOPA-evoked rhythm (Fig. 9b) as has been shown in cats[39].

Intracellular recording techniques can be combined with ENG recordings to observe the activity of single neurons during locomotor-like activity (Fig. 9c). The neurons fire action potentials during the activity phase on the corresponding nerve and are usually silent when the corresponding ENG is silent. The firing frequency for the neuron varies throughout its active phase and invariably matches the ENG activity in the corresponding nerve. The firing patterns vary from cell to cell but generally show a decrementing firing pattern during the active phase (two-thirds of motoneurons, Fig. 9d,g), starting with high firing frequencies and decreasing. Incrementing firing patterns (Fig. 9e) and incrementing–decrementing ramps are occasionally observed but are rare. The maximum firing frequencies recorded during the active phase range from 86 Hz to 356 Hz (mean 178 Hz), and the minimum firing frequencies during the active phases range from 11 Hz to 83 Hz (mean 26 Hz). In just over half of cells, the onset of firing in the active phase occurred in the form of doublets or triplets (or even quadruplets, Fig. 9g). These had an interspike interval of between 2.6 and 11 ms, followed by a prolonged interspike interval, as has been described for other species. In just over half of the motoneurons, clear periods of pronounced inhibition were observed during periods of activity on the antagonist nerve ENG (Fig. 9d,e,f). The degree of inhibition matched the degree of activity in the antagonist nerve, suggesting a common drive to both motoneurons and to interneurons inhibiting antagonist motoneurons (reciprocal inhibition) during L-DOPA-evoked locomotion in mice.

Actual stepping preparation

Historically, decerebrate nonparalyzed cats walking on treadmills have been used to demonstrate the influence of afferent feedback on the locomotor pattern. This is also possible in nonparalyzed mice. After decerebration and discontinuation of anesthesia, we observed that within 10–30 min an increase in muscle tone and reflex responses occurred (Supplementary Fig. 2). The increase in muscle tone, evident by an increase in EMG activity (Fig. 11a), could be visualized as an increase in weight support. This increase in activity would prompt the experimenter to start the treadmill, and, with practice, stepping could be routinely elicited from decerebrate mice. This is in contrast to fictive locomotion, where bouts of non-drug-evoked locomotion were rare—although afferent nerve stimulation can evoke rhythmic alternating activity of flexor and extensor nerves. Although treadmills can be used, decerebrate mice can also locomote well over a wheel, which in our case was manufactured out of light-weight Styrofoam (Fig. 11b). The advantage of this setup is that spontaneous bouts of locomotion can be recorded in which the mouse runs at its own speed or by motorizing the wheel with a simple clutch mechanism. Supplementary Video 1 shows an example of stepping using this apparatus. Figure 11c,d illustrates the various data types that can be recorded simultaneously from a decerebrate mouse preparation. The wheel can be adapted to fix the spinal cord for extracellular recordings. Compared with freely behaving mice, decerebrate mice allow for more invasive procedures to be used. For example, limbs

can be partially fixed in place[40], optical recording and stimulation techniques can be more easily deployed, and the effects of acute transections of the spinal cord can be assessed[41].

Optogenetics

A clear potential for the use of the preparation is the use of optogenetic approaches to examine activation and inactivation of specific neurons within the spinal cord (Fig. 12). We show here an example of photostimulation of VGAT neurons in the spinal cord to depress activation of the H-reflex recorded from the flexor digitorum brevis—which functions to measure the monosynaptic stretch reflex; such photostimulation can be achieved using a custom-made micro-LED array implanted over the dorsal surface of the spinal cord. This device also potentially can be used in stepping animals.

Conclusion

The decerebrate preparation can be used to both examine stepping behavior and record from motoneurons and candidate interneurons in the spinal cord. These procedures can be adapted to record from intra-axonal afferents and motor units. Although the examples are from the hind-limb motor system, the decerebrate model described here can be easily adapted for use in respiratory studies, cardiovascular function, and pain studies, for example.

Supplementary Material

Refer to Web version on PubMed Central for supplementary material.

ACKNOWLEDGMENTS

This work was supported by Natural Sciences and Engineering Research Council grants to P.J.W. M.M. received funds from NIH NINDS R01NS077863. C.F.M. received funds from an EU FP7 Marie Curie Fellowship and project grants from the Lundbeck Foundation.

C.F.M. acknowledges the technical assistance of L. Grøhndahl of the Meehan laboratory, the assistance of A. Hedegaard of the Meehan laboratory for the voltage clamp experiments, and advice regarding the voltage clamp and the voltage clamp external gain instrument from C.J. Heckman (Northwestern University). K.A.M. received a studentship from the Branch Out Neurological Foundation and the Hotchkiss Brain Institute. P.J.W. and K.A.M. acknowledge the technical assistance of A. Krajacic of the Whelan laboratory.

References

1. Kiehn O Development and functional organization of spinal locomotor circuits. Curr. Opin. Neurobiol 21, 100–109 (2011). [PubMed: 20889331]
2. Grossmann KS, Giraudin A, Britz O, Zhang J & Goulding M Genetic dissection of rhythmic motor networks in mice. Prog. Brain Res 187, 19–37 (2010). [PubMed: 21111198]
3. Whelan PJ Shining light into the black box of spinal locomotor networks. Philos. Trans. R. Soc. Lond. B Biol. Sci 365, 2383–2395 (2010). [PubMed: 20603359]
4. Dougherty KJ et al. Locomotor rhythm generation linked to the output of spinal shox2 excitatory interneurons. Neuron 80, 920–933 (2013). [PubMed: 24267650]
5. Lanuza GM, Gosgnach S, Pierani A, Jessell TM & Goulding M Genetic identification of spinal interneurons that coordinate left-right locomotor activity necessary for walking movements. Neuron 42, 375–386 (2004). [PubMed: 15134635]
6. Bretzner F & Brownstone RM Lhx3-Chx10 reticulospinal neurons in locomotor circuits. J. Neurosci 33, 14681–14692 (2013). [PubMed: 24027269]

7. Mendelsohn AI, Simon CM, Abbott LF, Mentis GZ & Jessell TM Activity regulates the incidence of heteronymous sensory-motor connections. Neuron 87, 111–123 (2015). [PubMed: 26094608]
8. Hägglund M et al. Optogenetic dissection reveals multiple rhythmogenic modules underlying locomotion. Proc. Natl. Acad. Sci. USA 110, 11589–11594 (2013). [PubMed: 23798384]
9. Wyart C et al. Optogenetic dissection of a behavioural module in the vertebrate spinal cord. Nature 461, 407–410 (2009). [PubMed: 19759620]
10. Goulding M, Bourane S, Garcia-Campmany L, Dalet A & Koch S Inhibition downunder: an update from the spinal cord. Curr. Opin. Neurobiol 26, 161–166 (2014). [PubMed: 24743058]
11. Akay T, Tourtellotte WG, Arber S & Jessell TM Degradation of mouse locomotor pattern in the absence of proprioceptive sensory feedback. Proc. Natl. Acad. Sci. USA 111, 16877–16882 (2014). [PubMed: 25389309]
12. Whelan PJ Developmental aspects of spinal locomotor function: insights from using the *in vitro* mouse spinal cord preparation. J. Physiol 553, 695–706 (2003). [PubMed: 14528025]
13. Schmidt BJ & Jordan LM The role of serotonin in reflex modulation and locomotor rhythm production in the mammalian spinal cord. Brain Res. Bull 53, 689–710 (2000). [PubMed: 11165804]
14. Mentis GZ, Alvarez FJ, Shneider NA, Siembab VC & O'Donovan MJ Mechanisms regulating the specificity and strength of muscle afferent inputs in the spinal cord. Ann. N. Y. Acad. Sci 1198, 220–230 (2010). [PubMed: 20536937]
15. Mentis GZ, Siembab VC, Zerda R, O'Donovan MJ & Alvarez FJ Primary afferent synapses on developing and adult Renshaw cells. J. Neurosci 26, 13297–13310 (2006). [PubMed: 17182780]
16. Meehan CF, Sukiasyan N, Zhang M, Nielsen JB & Hultborn H Intrinsic properties of mouse lumbar motoneurons revealed by intracellular recording *in vivo*. J. Neurophysiol 103, 2599–2610 (2010). [PubMed: 20164401]
17. Manuel M et al. Fast kinetics, high-frequency oscillations, and subprimary firing range in adult mouse spinal motoneurons. J. Neurosci 29, 11246–11256 (2009). [PubMed: 19741131]
18. Meehan CF et al. Intrinsic properties of lumbar motor neurones in the adult G127insTGGG superoxide dismutase-1 mutant mouse *in vivo*: evidence for increased persistent inward currents. Acta Physiol 200, 361–376 (2010).
19. Kleiber M Body size and metabolic rate. Physiol. Rev 27, 511–541 (1947). [PubMed: 20267758]
20. Nakanishi ST & Whelan PJ A decerebrate adult mouse model for examining the sensorimotor control of locomotion. J. Neurophysiol 107, 500–515 (2012). [PubMed: 21994265]
21. Meehan CF, Grondahl L, Nielsen JB & Hultborn H Fictive locomotion in the adult decerebrate and spinal mouse *in vivo*. J. Physiol 590, 289–300 (2012). [PubMed: 22106172]
22. Iglesias C et al. Mixed mode oscillations in mouse spinal motoneurons arise from a low excitability state. J. Neurosci 31, 5829–5840 (2011). [PubMed: 21490224]
23. Delestrée N et al. Adult spinal motoneurones are not hyperexcitable in a mouse model of inherited amyotrophic lateral sclerosis. J. Physiol 592, 1687–1703 (2014). [PubMed: 24445319]
24. Hedegaard A et al. Postactivation depression of the Ia EPSP in motoneurons is reduced in both the G127X SOD1 model of amyotrophic lateral sclerosis and in aged mice. J. Neurophysiol 114, 1196–1210 (2015). [PubMed: 26084911]
25. Lehnhoff J, Moldovan M, Hedegaard LG & Meehan CF *In vivo* intracellular recordings from spinal lumbar motoneurones in P0-deficient mice indicate an activity-dependent axonal conduction failure in otherwise functional motoneurones. Proc. Physiol. Soc 31, PCA079 (2014).
26. Alstermark B & Ogawa J recordings of bulbospinal excitation in adult mouse forelimb motoneurons. J. Neurophysiol 92, 1958–1962 (2004). [PubMed: 15084639]
27. Wilson RJA, Chersa T & Whelan PJ Tissue PO2 and the effects of hypoxia on the generation of locomotor-like activity in the *in vitro* spinal cord of the neonatal mouse. Neuroscience 117, 183–196 (2003). [PubMed: 12605904]
28. Husch A, Dietz SB, Hong DN & Harris-Warrick RM Adult spinal V2a interneurons show increased excitability and serotonin-dependent bistability. J. Neurophysiol 113, 1124–1134 (2015). [PubMed: 25520435]

29. Mitra P & Brownstone RM An *in vitro* spinal cord slice preparation for recording from lumbar motoneurons of the adult mouse. J. Neurophysiol 107, 728–741 (2012). [PubMed: 22031766]
30. Husch A, Cramer N & Harris-Warrick RM Long-duration perforated patch recordings from spinal interneurons of adult mice. J. Neurophysiol 106, 2783–2789 (2011). [PubMed: 21900514]
31. Bennett DJ, Li Y & Siu M Plateau potentials in sacrocaudal motoneurons of chronic spinal rats, recorded *in vitro*. J. Neurophysiol 86, 1955–1971 (2001). [PubMed: 11600653]
32. Long SK, Evans RH, Cull L, Krijzer F & Bevan P An *in vitro* mature spinal cord preparation from the rat. Neuropharmacology 27, 541–546 (1988). [PubMed: 3393270]
33. Jiang MC & Heckman CJ *In vitro* sacral cord preparation and motoneuron recording from adult mice. J. Neurosci. Methods 156, 31–36 (2006). [PubMed: 16574242]
34. Silverman J, Suckow MA & Murthy S The IACUC Handbook 3rd edn. (CRC Press, 2014).
35. Carlin KP, Jiang Z & Brownstone RM Characterization of calcium currents in functionally mature mouse spinal motoneurons. Eur. J. Neurosci 12, 1624–1634 (2000). [PubMed: 10792440]
36. Heckman C & Lee R Advances in measuring active dendritic currents in spinal motoneurons. in Motor Neurobiology of the Spinal Cord (ed. Cope TC) 89–105 (CRC Press, 2001).
37. Lee RH & Heckman CJ Bistability in spinal motoneurons *in vivo*: systematic variations in persistent inward currents. J. Neurophysiol 80, 583–593 (1998). [PubMed: 9705452]
38. Jordan LM, Liu J, Hedlund PB, Akay T & Pearson KG Descending command systems for the initiation of locomotion in mammals. Brain Res. Rev 57, 183–191 (2008). [PubMed: 17928060]
39. Conway BA, Hultborn H & Kiehn O Proprioceptive input resets central locomotor rhythm in the spinal cat. Exp. Brain Res 68, 643–656 (1987). [PubMed: 3691733]
40. Duysens J & Pearson KG Inhibition of flexor burst generation by loading ankle extensor muscles in walking cats. Brain Res 187, 321–332 (1980). [PubMed: 7370733]
41. Whelan PJ Control of locomotion in the decerebrate cat. Prog. Neurobiol 49, 481–515 (1996). [PubMed: 8895997]

Box 1 |

Nerve dissection for intracellular recordings and fictive locomotion ● TIMING 15 min

Additional materials required:

- Blunt-tipped scissors (Fine Science Tools, cat. no. 14072-10)
- Bipolar hook electrodes (custom made, see Fig. 6b)
- Constant-voltage isolated stimulator (AMPI ISO-Flex)

Procedure

1. Completely shave one hind limb.
2. Using a no. 10 round-blade scalpel, cut the skin of the hind limb from the hip joint to the ankle, then expose the lateral muscles using blunt-tipped scissors. The edge of the biceps femoris muscle, where the gluteal muscles intersect, should be visible as a thin white line (Fig. 5a).
3. Using fine scissors, cut along this white line from the knee to the hip.

   ▲ **CRITICAL STEP** There are many superficial blood vessels in the hind limbs; use precautions to avoid cutting blood vessels close to the knee or close to the hip to avoid blood loss. Use a hand-held cauterizer as needed, but never use it too close to the nerves.
4. Cut the biceps femoris along the tibia.
5. Pull the biceps femoris up to expose the sciatic nerve and, using blunt forceps, dissect the nerve from the surrounding connective tissue (Fig. 5b–c).

   ▲ **CRITICAL STEP** The biceps can be resected completely or simply dissected to the side at this point.

   ▲ **CRITICAL STEP** The sciatic nerve has been used here as an example; the various branches of the sciatic nerve can be individually dissected, cut, and placed on bipolar stimulation electrodes for antidromic identification of pools of motoneurons.
6. Tie the leg to the custom-made leg holder with a thread attached to the ankle and place a pin through the knee joint and into the leg holder. This easily constructed leg holder allows the skin to be pinned to the holes in the side to create a leg pool, which can be filled with paraffin oil to keep the muscle and nerves moist and at the correct temperature (Fig. 6a, Supplementary Fig. 1b).

   ▲ **CRITICAL STEP** It is important to regularly monitor the temperature of the leg oil pool independently of the core temperature, as even small drops in temperature can substantially affect force recordings and conduction velocity.

7. Using bipolar hook electrodes (custom made, see Fig. 6b), hang the nerve into the hook (Fig. 6b) and connect to a constant-voltage isolated stimulator (AMPI ISO-Flex).

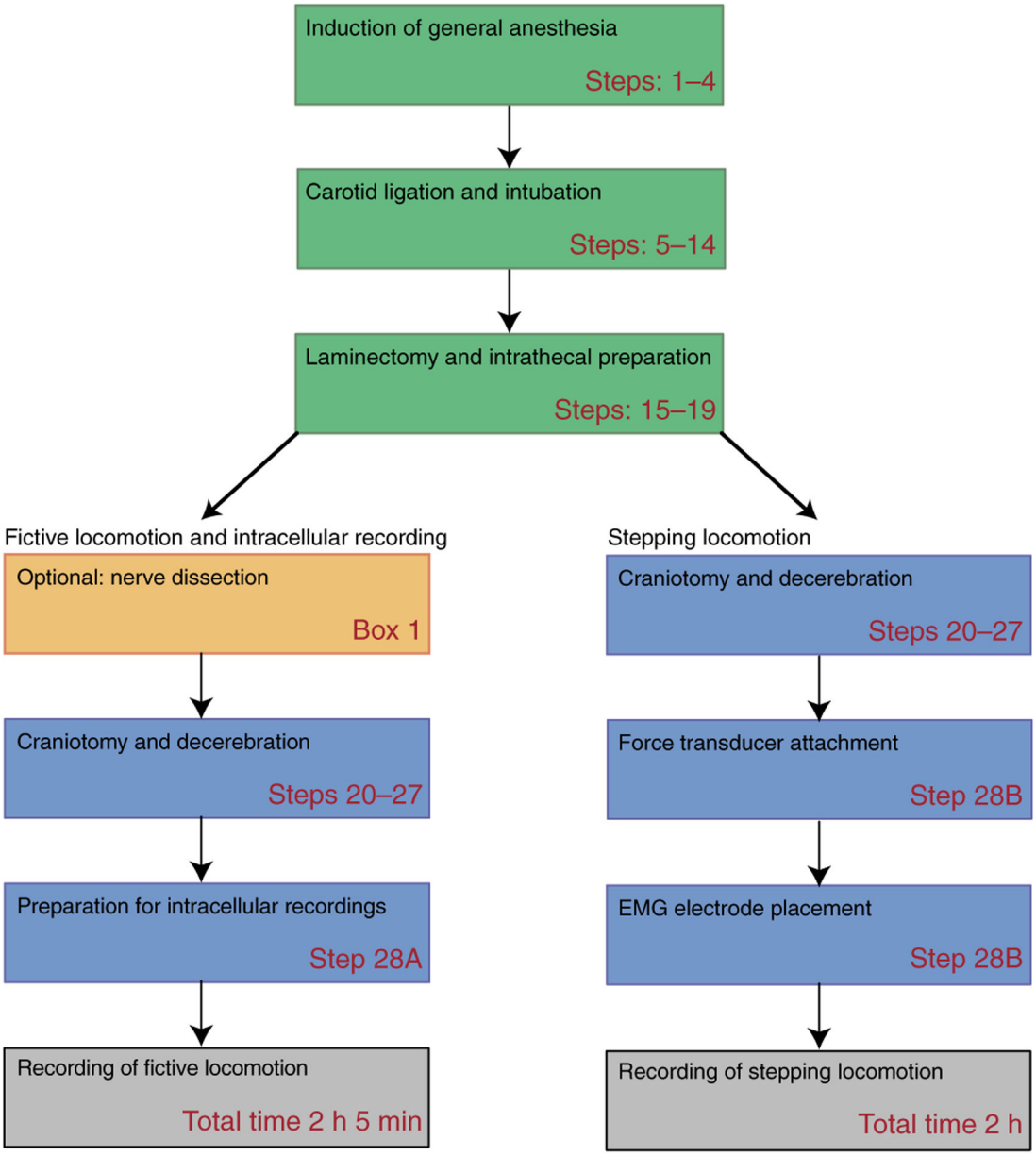

Figure 1 |.

Procedural steps for creating a decerebrate preparation. Schematic block representation of decerebration procedure and steps to create a fictive or actual stepping preparation. The step numbers refer to the Procedure steps in the protocol.

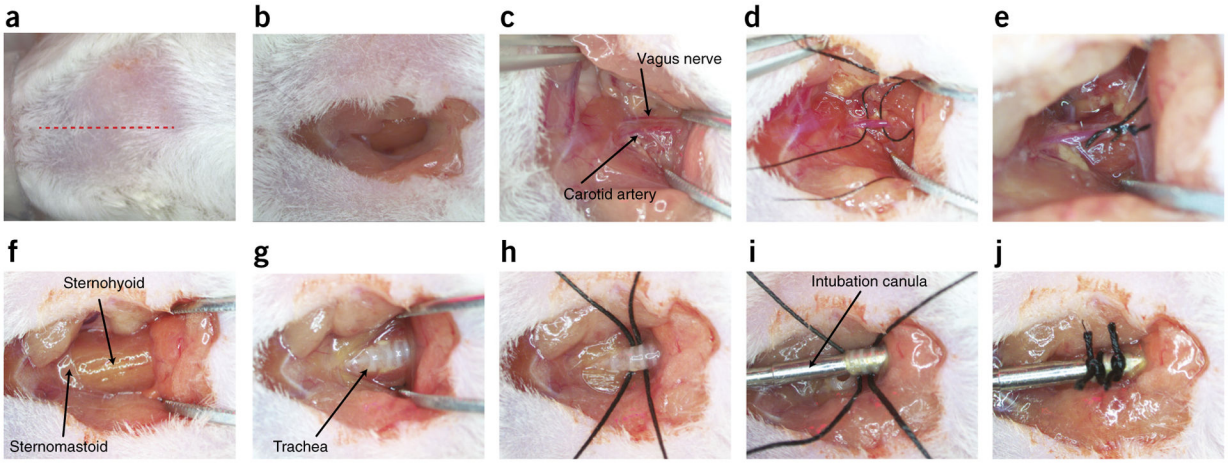

Figure 2 |.

Surgical preparation of carotid to artery ligation and tracheotomy. (**a**) Red dotted line indicates location of superficial cut along the midline of the neck. (**b**) Excavation of the superficial adipose tissue to expose the sternohyoid muscles. (**c**) Blunt dissection of the carotid artery and vagus nerve. (**d**) 6-0 sutures run underneath the carotid artery, avoiding the vagus nerve. (**e**) Unilateral tied sutures of the carotid artery. (**f**) Location of sternohyoid and sternomastoid muscles. (**g**) Separation of the sternohyoid muscle to expose the trachea. (**h**) 4-0 sutures run under the trachea for future use. (**i**) Tracheal cannula inserted into the trachea. (**j**) Tracheal cannula sutured into place for attaching to a ventilator. Local ethics committees approved the procedures shown here. This figure illustrates Steps 5–14 of the PROCEDURE.

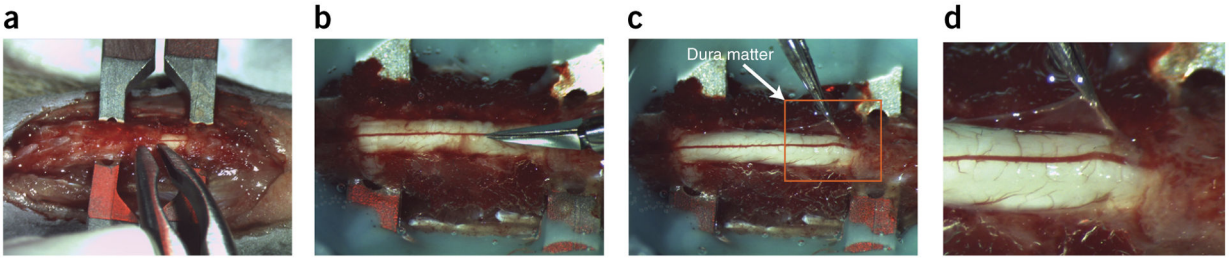

Figure 3 |.

Laminectomy with durotomy. (**a**) Representation of a three-vertebra laminectomy with dura mater attached. Rongeurs or laminectomy forceps are used to clip away the lamina. (**b**) Spinal cord with the dura mater in the process of being opened with small spring scissors. (**c**) The dura—held by forceps. **(d)** Close-up view of the image within the orange square in **c**. This laminectomy is suitable for application of substances and optogenetics, but smaller laminectomies can improve stability of the spinal cord, which is useful for intracellular recordings. This figure illustrates Steps 15–17 of the PROCEDURE. Local ethics committees approved the procedures shown here.

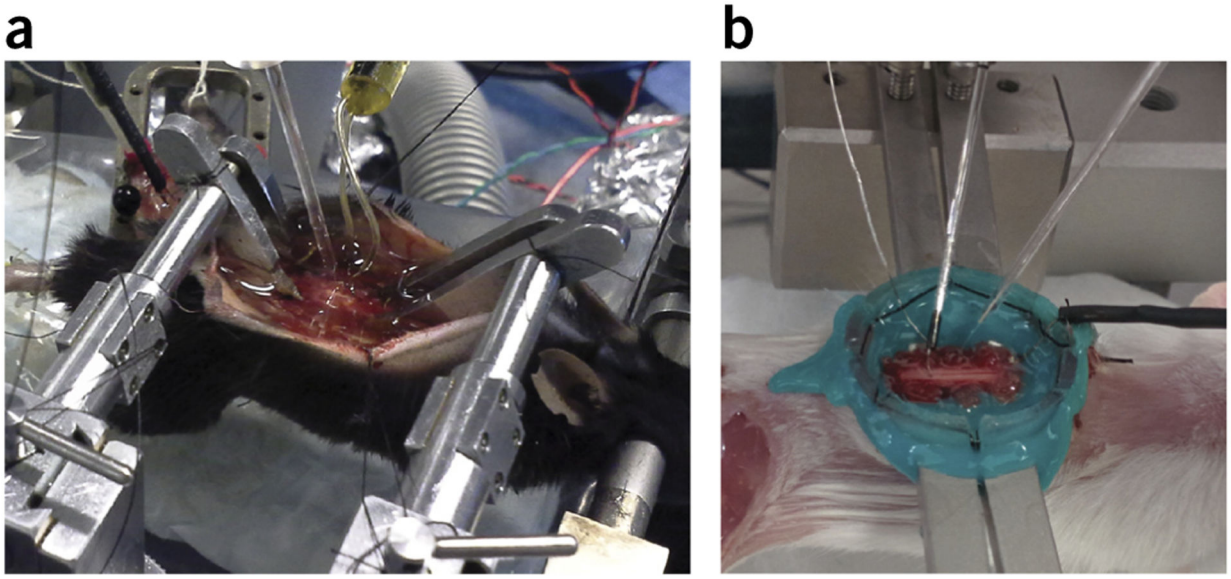

Figure 4 |.

Intracellular recording and antidromic stimulation. (**a**) Intracellular recording setup as viewed from the right side of the animal, showing the use of Narashige clamps, which provides an excellent range of motion. (**b**) Alternative setup showing the use of Cunningham spinal clamps, which provides for greater working space on the dorsal surface due to the lateral placement of clamps. This figure illustrates to Step 18A of the PROCEDURE. Local ethics committees approved all procedures shown here.

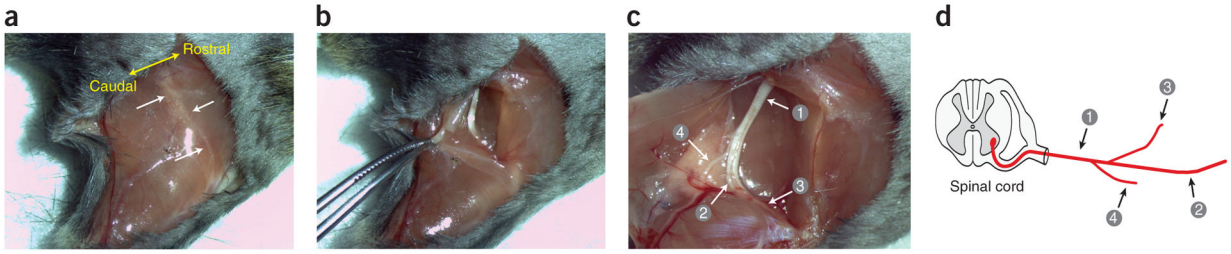

Figure 5 |.

Sciatic nerve isolation of the hind limb. (**a**) Superficial cut starting at the hip joint, proceeding straight to the knee joint and ending at the ankle joint. The location of the intersection point between the gluteal muscles and the biceps femoris is indicated by a thin white line in the tissue. White arrows identify muscle facia, and yellow arrow indicates the rostro-caudal orientation of the mouse. (**b**) Dissection of the gluteal muscles and the biceps femoris after cutting along the connecting line. (**c**) Visualization of the (1) sciatic nerve and the nerve branches consisting of the (2) tibial, (3) common peroneal, and (4) sural nerves. (**d**) The various branches of sciatic nerve shown in schematic form. Local ethics committees approved all procedures shown here.

See REAGENTS section for details. This figure to illustrates Box 1, steps 1–5. Local ethics committees approved the procedures shown here.

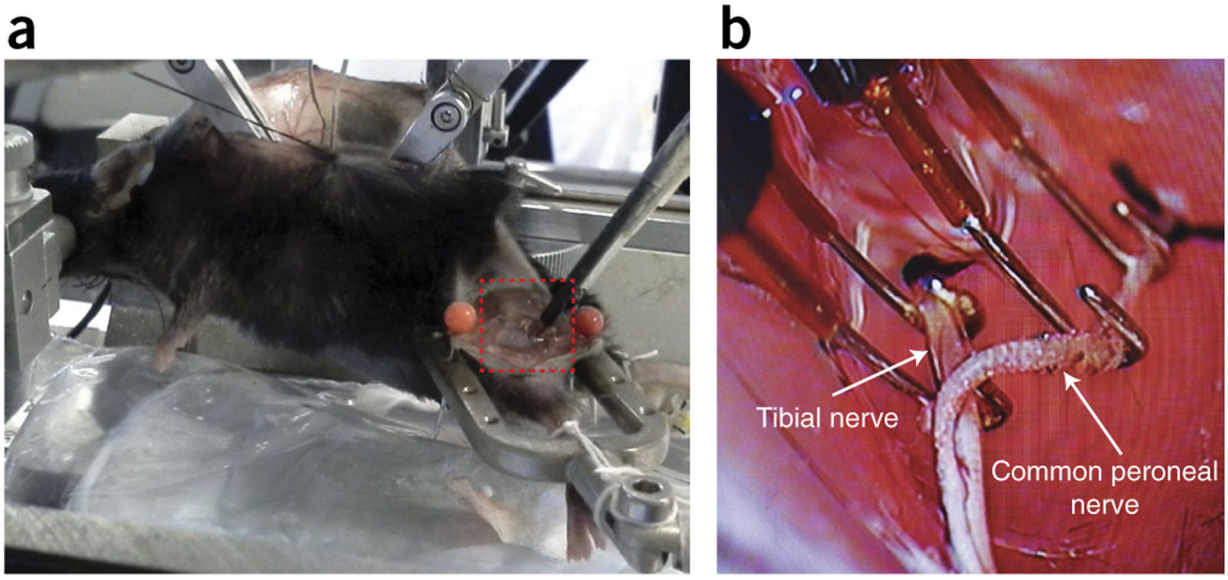

Figure 6 |.

Hind-limb securing and antidromic stimulation of nerves. (**a**) Hind-limb stimulation. Left hind limb is secured in a custom-made holder with nerves dissected. Red dashed box indicates the placement of hook electrodes with oil bath. (**b**) Stimulating hook electrodes (close-up view of the area outlined by the dashed red box in **a**). Two sets of hook electrodes are placed under the tibial nerve and common peroneal nerve for evoking antidromic action potentials. See REAGENTS section for details. This figure illustrates Box 1, steps 6 and 7. Local ethics committees approved all procedures shown here.

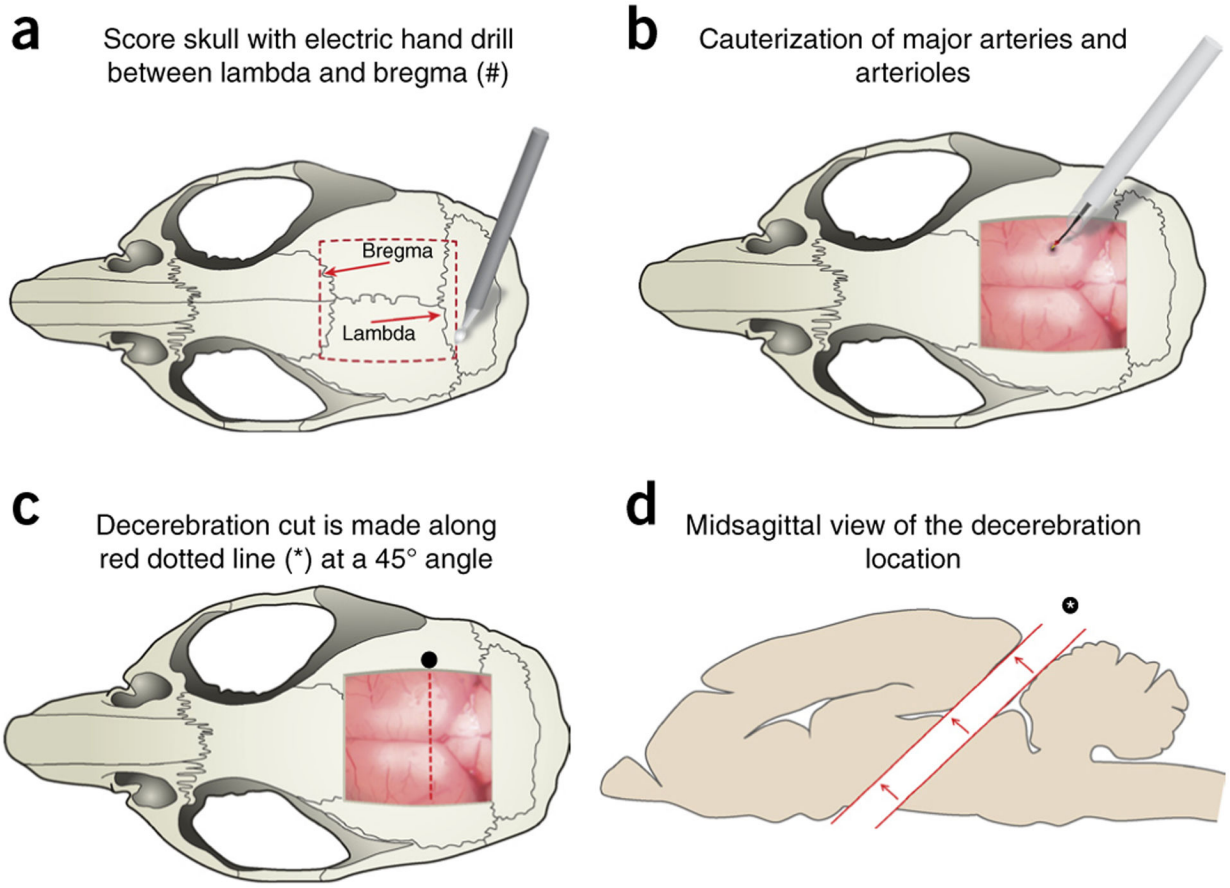

Figure 7 |.

Craniotomy and decerebration cut location. (**a**) Craniotomy and brain exposure are performed by first scoring a square outline (red dashed box) between the lambda and the bregma using an electric handheld drill. The mouse rongeur tool is used to remove the skull as one piece by lifting the scored area, exposing the brain and meninges. (**b**) Superior sagittal sinus vein and other major vasculature are cauterized using hand cauterization tool (Acu-Tip Portable or Bovie Change-A-Tip) at the most caudal end to reduce bleeding. (**c**) Schematic representation of the removal of the cerebral cortex (decerebration) and underlying structures. Decerebration is performed with a no. 10 round blade, cutting through the brain at a 45° angle; cut is represented by an asterisk and the red dotted line. (**d**) Rostral portion of brain is carefully removed from the cut (asterisk) using a microspatula and without damage to the remaining caudal section. In the absence of the rostral brain, the remaining cavity is filled with a hemostatic sponge and/or Surgicel. This figure illustrates Steps 20–27 of the PROCEDURE. Local ethics committees approved all procedures shown here.

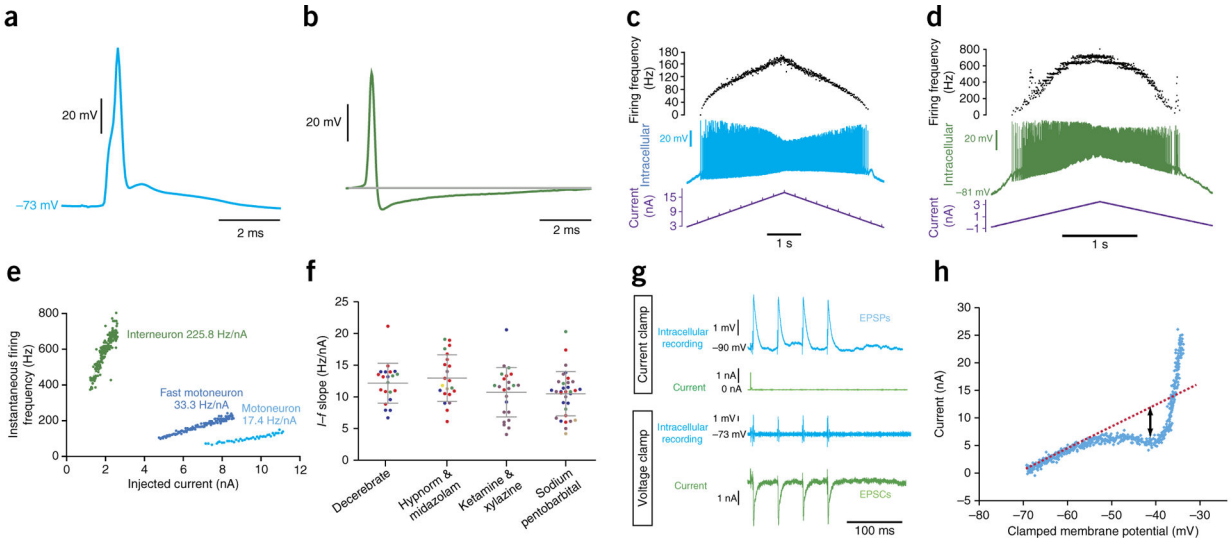

Figure 8 |.

Comparison of intracellular recordings from a motoneuron and a candidate interneuron. These intracellular recordings were performed in adult female C57BL/6J mice, and all recordings in decerebrates were performed at least 2 h after removal of isoflurane from the ventilation flow, to allow for metabolism of the isoflurane. (**a**) Average antidromic action potentials ($n = 18$) from stimulation of the sciatic nerve, recorded from a motoneuron in a decerebrate mouse. (**b**) An average of six spontaneous action potentials recorded in a candidate ventral horn interneuron in an anesthetized mouse. (**c**) Repetitive firing (middle trace) evoked in a motoneuron in a decerebrate mouse following intracellular ramp current injection (lower trace). Upper trace shows instantaneous firing frequency. (**d**) Repetitive firing evoked (middle trace) in the same interneuron as in **b**, following intracellular current injection (lower trace). Upper trace shows instantaneous firing frequency. (**e**) Graph showing an example *I–f* slope obtained for a ventral horn interneuron (green) in a mouse. This can be compared with an example of a typical *I–f* slope from a mouse motoneuron (light blue) and an example of one of the steepest *I–f* slopes that we have recorded over the years (from a presumptive fast motoneuron, darker blue). (**f**) Comparison of current–frequency (*I–f*) slopes recorded from individual motoneurons (single dots) in decerebrate mice and in mice under different anesthesia types ($n = 99$ motoneurons (decerebrate $n = 21$ cells from 3 mice, Hypnorm & midazolam $n = 21$ cells from 5 mice, ketamine & xylazine $n = 24$ cells from 4 mice, sodium pentobarbital $n = 33$ cells from 5 mice; a total of 18 mice were used)). Horizontal lines and error bars represent mean ± s.d. Cells from individual mice within each group are color-coded. The data in this figure come from a series of experiments designed specifically to compare *I–f* slopes in decerebrate mice with those of anesthetized mice and so all parameters were kept constant (and the examples from **e** are not included). (**g**) Current clamp (upper two traces) and voltage clamp (lower two traces) of a series of intracellular recorded EPSPs in an adult mouse spinal motoneuron *in vivo* evoked by stimulation of the tibial nerve. (**h**) The *I–V* function recorded under voltage clamp during a voltage ramp command. A negative inflection is seen at ~−53 mV, consistent with the onset of persistent inward currents calculated by measuring the deviation of the negative slope region from

the theoretical line expected without their activation. Local ethics committees approved all procedures used to obtain these results. See REAGENTS section for details.

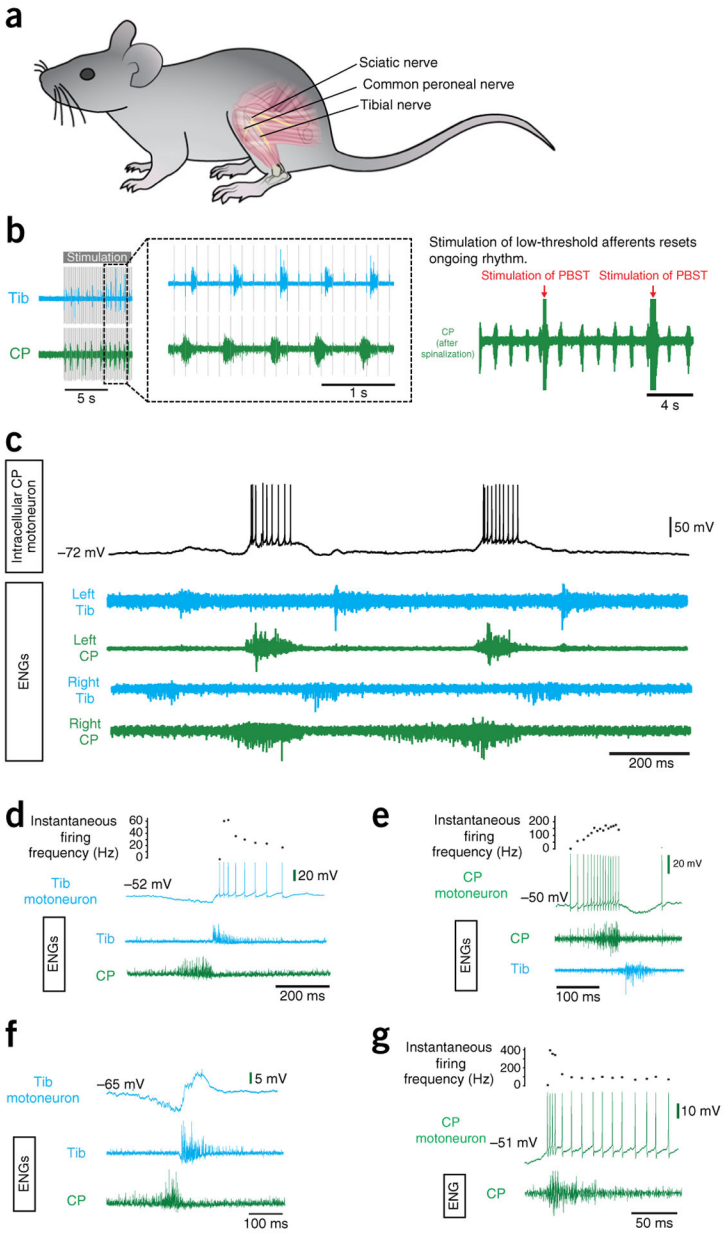

Figure 9 |.

Evoking fictive locomotion in a decerebrate mouse after L-DOPA treatment. (**a**) Schematic illustrating the spinal cord and the dissected peripheral nerve branches of the sciatic nerve: the common peroneal (CP) and tibial (Tib) nerves. (**b**) The effects of peripheral nerve stimulation. Left: an example of rhythmic activity evoked by peripheral nerve stimulation (tested after L-DOPA administration and before spontaneous L-DOPA locomotion started). Right: once the L-DOPA-induced rhythm develops, the rhythm can be reset by stimulation of a peripheral nerve (in this case the nerve branches innervate posterior biceps and semitendinosus (PBST) muscles). In this example, the rhythm was enhanced by a rostral spinalization. (**c**) Intracellular recording from a CP motoneuron (upper trace) during a period of L-DOPA-evoked fictive locomotion. This is depicted as rhythmic ENG activity (lower

traces) alternating between nerves innervating flexor muscles (CP) and nerves innervating extensor muscle (Tib) extensor on a single side. (**d**) An example of a recording from a Tib motoneuron showing a decrementing pattern of discharge during the active phase on the corresponding ENG recorded from the Tib nerve. Note the inhibition of the V_m of the motoneuron during the active phase of the antagonist nerve (CP). (**e**) An example of a recording from a CP motoneuron showing an incrementing pattern of discharge during the active phase on the corresponding CP ENG. Inhibition is also seen during the antagonist (Tib) ENG phase. (**f**) An example of a recording from a slightly more hyperpolarized Tib motoneuron, revealing a clear phase of inhibition and excitation during the active phases of the Tib and CP nerve ENG, respectively. (**g**) An example of a recording from a CP motoneuron showing an initial high-frequency burst of action potentials (a quadruplet) at spike onset, followed by a rapidly decrementing pattern. Local ethics committees approved all procedures used to obtain the results shown here. See REAGENTS section for details. ENG, electroneurogram.

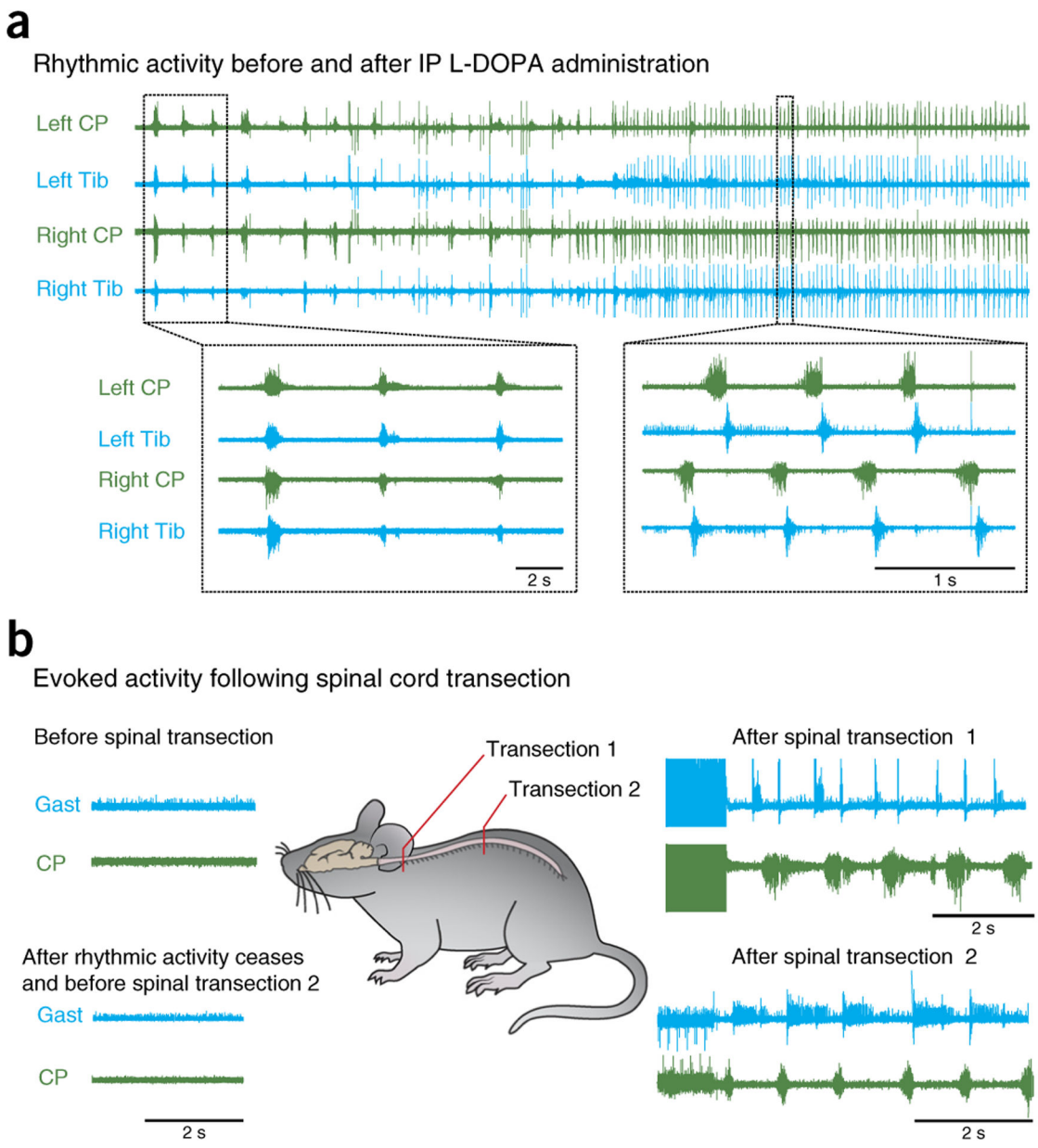

Figure 10 |.

Effect of spinalization on fictive locomotion. (**a**) Spontaneous locomotion recorded from common peroneal (CP) and tibial (Tib) ENGs after administration of L-DOPA. Lower left insert shows zoomed in section illustrating slow synchronous activity on all nerves. Lower right insert shows a time period later in the recording, at which the activity on all nerves is faster, with alternation between left and right legs and flexor and extensors. (**b**) An example of the effect of spinalization on rhythmic activity. L-DOPA-induced locomotion had ceased. A spinalization at the cervical level resulted in rhythmic activity between the flexor nerve, CP, and the extensor nerve, gastrocnemius (Gast). Once locomotion ceased, it could be elicited again by a second thoracic spinal transection. Local ethics committees approved all procedures used to produce data shown here.

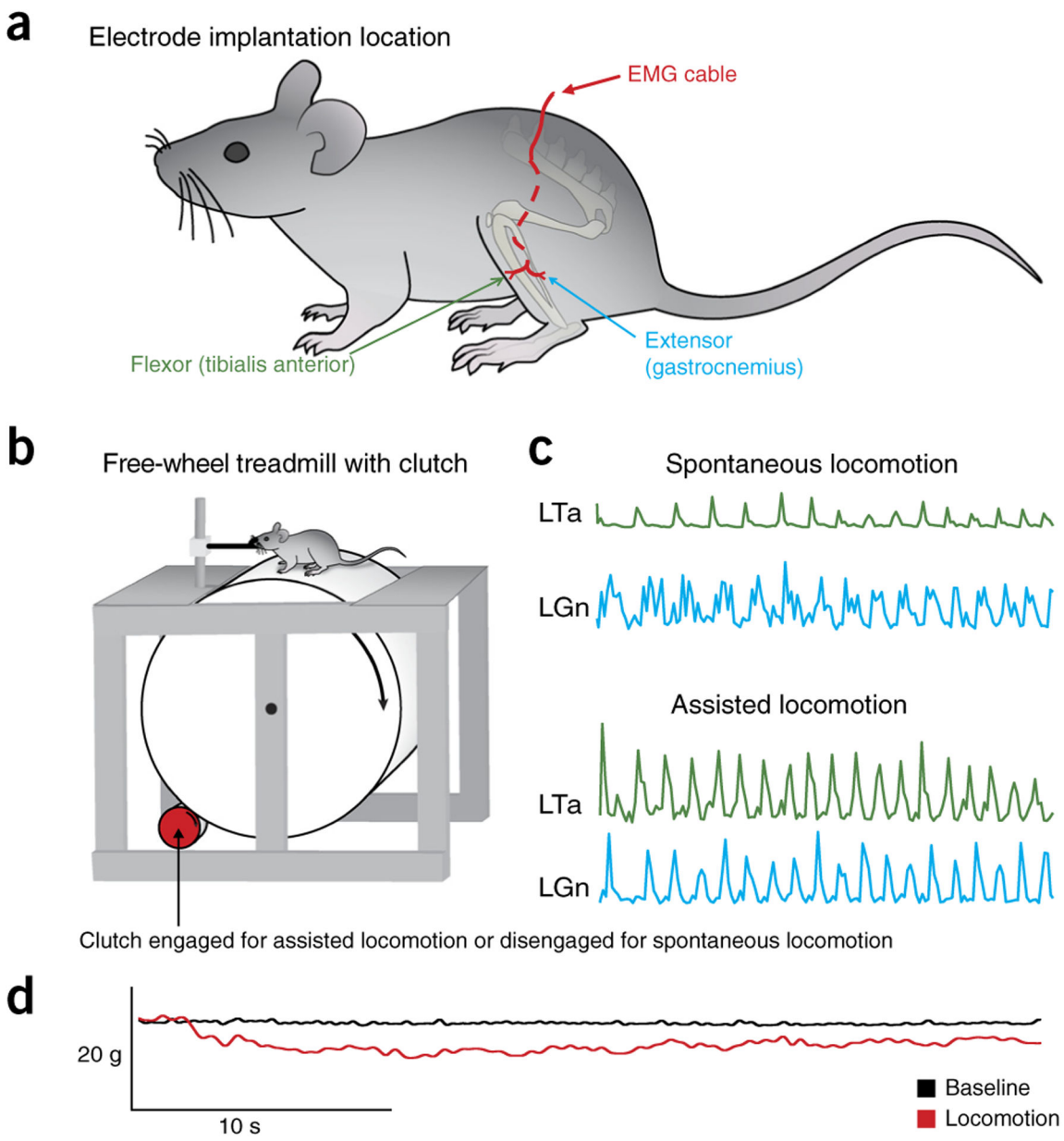

Figure 11 |.

Assisted and spontaneous locomotion evoked on clutch-driven treadmill. (**a**) Schematic representation of the left side of the mouse, with EMG electrode insertion into the tibialis anterior and gastrocnemius muscles. The EMG cable is secured subcutaneously to reduce EMG motion artifacts. (**b**) Schematic of the free-wheel treadmill with clutch system allowing for spontaneous and assisted treadmill locomotion. (**c**) Example traces of spontaneous and assisted locomotion from CFW decerebrate mice—EMG traces were recorded from the left tibialis anterior (LTa) and gastrocnemius (LGn). (**d**) Example trace of a 40-s bout of locomotion demonstrating the weight-bearing at baseline compared with weight-bearing during intrathecal administration of dopamine using a force transducer. Weight change in the force transducer is inversely proportional to the weight-bearing by the

mouse. The black bars indicate the stance phase of the left and right limbs. Local ethics committees approved all procedures used to produce data shown here. See REAGENTS section for details. Figure 11 refers to Step 28B of the PROCEDURE.

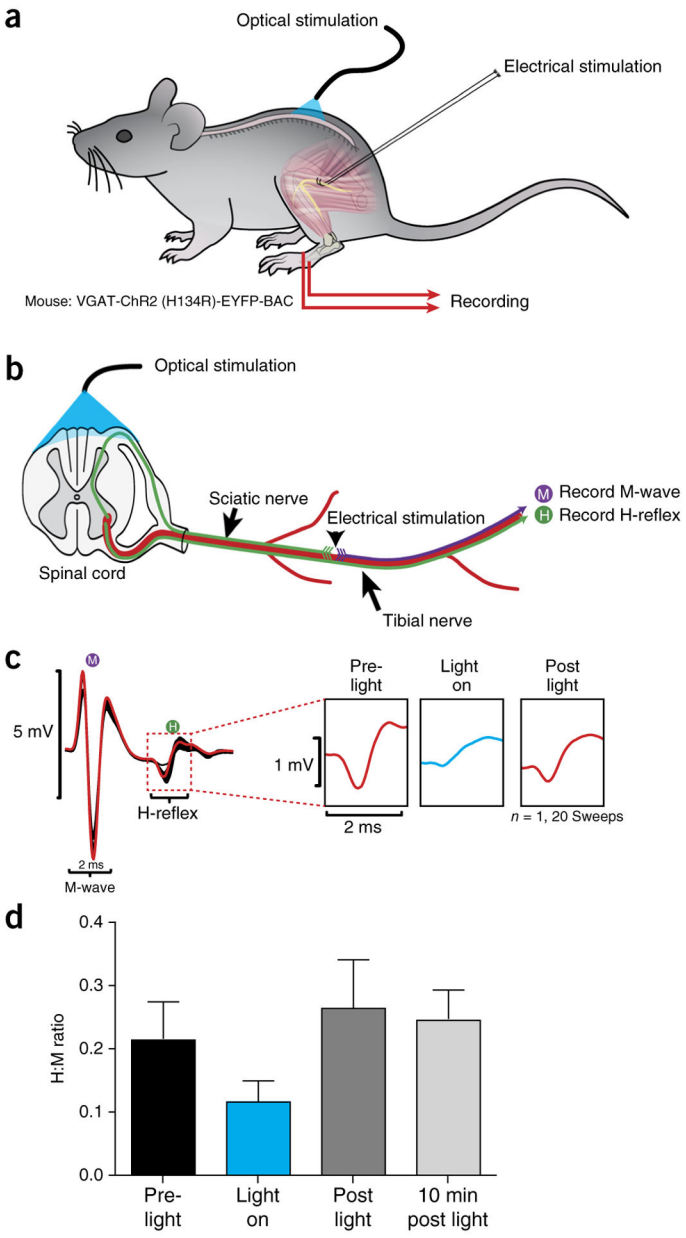

Figure 12 |.

Photostimulation of the dorsal L4/L5 spinal cord reduces amplitude of monosynaptic reflex. (**a**) Schematic representation of stimulation and recording setup. (**b**) Electrical stimulation of the sciatic nerve was performed on VGAT-ChR2 (H134R)-EYFP-BAC mice in the presence and absence of trains of photostimulation targeted toward VGAT neurons in the spinal cord. Photostimulation was accomplished using an array of six micro-LEDs in a flexible silicone bilayer, allowing stimulation of the surface of the spinal cord. (**c**) Example traces show a reduction in the H-reflex recorded from the flexor digitorum brevis (marked H in diagram) and expanded in right panels to show reduction in the H-reflex amplitude during light-on conditions. (**d**) Graph summarizing effects across conditions. Error bars refer to mean ± s.d. $n = 20$ for each bar. Local animal ethics committees approved these procedures. See

REAGENTS section for details. Local ethics committees approved all procedures used to produce results shown here.

TABLE 1 |

Troubleshooting table

Step	Problem	Possible reason	Possible solution
4	Breathing is irregular	Isoflurane level is too high or low	Adjust isoflurane as needed
9	Breathing becomes slow and/or sporadic	Potential vagus nerve injury or ligation	Check to see whether the vagus nerve was ligated with the carotid artery. If yes, remove sutures and re-tie only the carotid artery Verify that the vagus nerve is not injured
12	Difficulty inserting tracheal cannula	Narrow trachea, large cannula	If the cannula is made of plastic, cut the tracheal cannula at an angle for easier insertion If the cannula is metal, use the end with the rounded edges for insertion
13	Ventilator is not providing flow	Tracheal cannula is blocked	Disconnect cannula from ventilator and check for blockages, verify air flow, and reconnect
14	Sudden change in CO_2 level	Temperature Tracheal tube movement—altering of dead space	Alter heat-lamp setting or proximity Check tubing—verify tracheal insertion
17	Excess bleeding during laminectomy	Ruptured vertebral arteries	Use bone wax or hemostatic sponges to minimize blood loss. The hemostatic sponges absorb the blood, quickly clearing the field of view and allowing the investigator to finish the laminectomy
23	Excessive blood loss during craniotomy	Vasculature of skull is bleeding	Use bone wax to seal the open bone vessels or hemostatic sponges to quickly clear the field of view while finishing the craniotomy
28A(ii)	Spinal cord is compressed by the intracellular electrode	Various	Adjust the shape of the electrode taper
	No incoming volley	Wrong spinal cord segment	Move recording electrode rostrally and caudally along the spinal cord to confirm. Verify the polarity of the stimulating electrodes to rule out anode block
28A(ix)	Field potential not visible	Incorrect placement of the electrode	Move the electrode in the rostro-caudal or mediolateral direction Change the angle of the electrode with respect to the vertical. The larger the angle, the more lateral the motoneuron pools targeted
28A(x)	Intracellular recordings are unstable	Movements of the vertebral column	Decrease the inspiration volume and adjust the other parameters to maintain adequate ventilation Improve fixation of the vertebral column on each side of laminectomy to prevent movements